# Segregation at Stacking Faults within the γ' Phase of Two Ni-Base Superalloys Following Elevated temperature Creep

**G.B. Viswanathan[1], A. Genc[2], V. Voronstrov[3], L. Kovarik[4], C. Rae[3] and M. J. Mills[1]**

## Introduction

Providing a complete understanding of the shearing of the strengthening γ' phase in Ni-base superalloys is essential for developing physics-based deformation models of these important materials for aerospace and power generations systems. The most widely accepted and employed shearing model is based on the premise that pairs of ½[110] matrix dislocations cooperatively shear the γ', necessitating the formation of an anti-phase boundary between these "superpartials." However, there is considerable evidence in the literature that shearing in the γ' phase occurs predominantly by formation of stacking faults (SISF and/or SESF) at intermediate temperatures under creep conditions [1-8]. The formation of these stacking faults are likely to be a key recovery process that relieve the build-up of dislocation content within the g channels.

Early work by Leverant and Kear [1], and later Rae and Reed [2], determined that both superlattice intrinsic and extrinsic (SISFs and SESFs) can be created in the γ'. In the instance of the "stacking fault ribbons," shearing occurs by the movement of an overall Burgers vector of a/2<112> dissociated into superlattice identical partial dislocations of the type 1/3<112> which individually dissociate into forming SISFs and SESFs. In the more recent work of Rae and Reed [3], the rate-limiting step for γ' shearing is the time-dependence due to waiting time at interfaces to form appropriate 1/3<112> dislocations for shearing to occur, for instance by the climb and reaction of different ½<110> matrix dislocations. Dislocations of the type 1/3<112> type have also been proposed to be the cause of nucleation of microtwins in CMSX-4 alloys at moderate temperatures. The models that propose shearing by 1/3<112> superpartial dislocations gained wide acceptance since this Burgers vector creates a stacking fault (local hexagonal stacking), but does not create first or second nearest neighbor violations of the ordered structure. Consequently, the formation of stacking faults and microtwins by this mechanism is a pure shear process that requires no long-range diffusion of atoms.

More recent studies have proposed that the elementary shearing process is actually due to the coordinated movement of 1/6<112> Shockley partials. For instance, based on detailed microscopy investigation, it has been proposed that SESFs, and microtwins that transcend both matrix and precipitates involve propagation of two closely separated 1/6<112> on consecutive (111) planes [4-6]. However, without any atomic rearrangement in the wake of these partials, a two layer complex stacking fault (CSF), or pseudotwin with passage of successive pairs of partials, would be formed due to the creation of wrong nearest neighbors. Since the energy of these faults should be very large, it has been further hypothesized that the rate of shearing by Shockley partial pairs is controlled by the elimination of the wrong nearest neighbors via local diffusion – a process termed "reordering." A quantitative model based on this hypothesis has been developed by

Kartikeyan, et al [7]. The diffusion mediated reordering process can convert the high energy two layer CSF into a low energy SESF. As this process occurs in the wake of the shearing partials, the forward movement of the partials is then controlled by the rate at which reordering can occur. Indeed, it has been proposed that the onset of reorder-mediated shearing determines the transition from the relatively athermal strength response of superalloys at lower temperatures, to the more temperature dependent behavior at intermediate temperatures. A detailed analysis of the possible atomic movements associated with such a reordering using VASP calculations has also been presented by Kovarik, et al [8].

In these previous studies, it has been assumed that the local composition at the faults remains constant, and that shearing/reordering involves only the rearrangement of atomic configurations adjacent to the faults in order to eliminate high energy, unfavorable nearest-neighbors. However, as pointed out first by Kovarik, et al [5], enhanced intensity of the atomic columns at SISF, SESF and twin boundaries is consistently observed using HAADF imaging, where the intensity is proportional to the $Z^{\sim 1.7-2}$. This consistent feature indicates possible segregation of heavier alloying atoms to these defects. Most recently, Vorontsov et al. [9] have also shown that both SISF and SESF faults show segregation of heavier elements in CMSX-4, indicating that diffusion-mediated segregation may also be an essential process controlling the γ' shearing at intermediate temperatures.

Although these HAADF results indicate higher Z element segregation to these faults, information concerning the segregating elemental species is presently lacking. This is mainly due to the following reasons. First, these faults are extremely thin; one or two atomic layers thick depending on whether they are SISF or SESF, respectively. This imposes limitations on the achievable resolution during EDS mapping. Second, the extremely low X-ray signals from these thin regions make it difficult to detect the segregation. These two problems are mitigated to a large extent in the present study since the analysis was conducted in the FEI 300 kV image corrected microscope that is capable of delivering 1.2A resolution in STEM. This resolution allows atomic scale imaging along close-packed zones required in this study where the 1-2 atomic layer thick faults are to be analyzed while oriented on their edge. Secondly, the ChemiSTEM technology allows collecting X-Ray counts in excess of 100 kcps from super EDS detectors and higher probe current.

In order to demonstrate the importance and possible universality of this segregation phenomena, results for two widely employed commercial superalloys following creep deformation are presented below. In the first, a polycrystalline sample of an advanced powder metallurgy alloy ME3 has been examined after tensile creep at 677°C and 724 MPa and a strain of ??%. The second sample is from a single crystal of CMSX-4 subjected to creep at a temperature of 750°C and a stress of 750 MPa with a tensile axis deviated from the [001] direction by 12.7° along an axis 24.4° from the (100) plane. This misalignment produces a single primary slip system having maximal Schmid factor for the [1-12](-111) slip system. The test was interrupted after 8.6% creep strain had been accumulated over 8 h. At the point of interruption, the material had completed primary creep and had been undergoing secondary creep for approximately 2 h. Additional information on the CMSX-4

testing can be obtained from reference [10]. TEM thin foils were extracted by cutting samples parallel to the tensile axis by spark erosion, and thin foils were prepared by subsequent electropolishing with a 6% perchloric acid solution in methanol (10% solution using 60% perchloric acid stock) at 18 V and -10°C. HR STEM imaging was performed on an image-corrected Titan G2 60-300 scanning transmission electron microscope (STEM) featuring a monochromator and equipped with FEI's ChemiSTEM technology. The compositional variations in the microstructure have been studied using the four-quadrant, FEI Super-X EDS detection system. The composition mapping was performed over an area of 200 x 200 nm area. The EDS spectrums were collected at an interval of 0.2 nm with drift correction in place.

Presented first are results for the alloy ME3 sample. In this sample, a number of faults within both the $\gamma$ and $\gamma'$ phases, as well as mictrotwins are observed. A grain near [1-10] orientation was selected for analysis. While in this alloy discriminating $\gamma$ and $\gamma'$ phases using HAADF is difficult due to the similar net atomic number of the two phases, and the relatively weak superlattice fringe contrast in the $\gamma'$, stacking faults in the $\gamma'$ are easy to identify because of the significantly enhanced Z-contrast. That this is contrast is indeed due to segregation can be verified by comparison of HAADF and low angle annular dark field (LAADF) images of the same fault. The enhanced intensity is observed only in the HAADF image, verifying that the contrast is not a diffraction effect, which would be enhanced in the LAADF image [11].

Figure 1a shows an HAADF image of an SISF oriented along [110] zone axis with the (1-11) fault plane parallel to the beam direction. Several elemental maps recorded from the same area are depicted Fig. 1a. The contrast in these images is qualitative since in some of the images the contrast was enhanced to illustrate the segregation effects. A number of interesting observations are made from these maps. The elements that are seen primarily richer on the fault itself are Co and Cr. On the other hand, Ni and Al were seen deficient on the stacking fault. Quantitative composition profiles for the same dataset are shown in Fig. 1b. In this analysis, the intensities are converted to mass fraction using the standard k factors for K$\alpha$ radiation for all elements except W and Ta. An accurate estimation of heavy elements such as W, Ta is expected to be unreliable since (i) their individual concentrations in this alloy is less than one percent and (ii) the K-peaks are not obtainable for these elements. As a result the estimation of these elements depends on the L and M lines. For alloys in this study, M peaks were preferred over L peaks since the latter ones were buried underneath the strong Ni-K$\beta$ peaks and the deconvolution of individual peaks would be difficult. In the case of Nb and Mo, L peaks were chosen over the K lines since the K peaks had lower intensities.

At each position shown in Fig. 1b, the intensities are integrated over a distance of 7 nm parallel to the fault in order to increase the signal to noise of the data. It can be seen that the principle results observed in the chemical maps are reinforced in the quantitative analysis, with Co and Cr clearly segregating to the fault, while Ni and Al are reduced locally. Note that the data are plotted on a logarithmic scale, so the reduction of Ni is much larger than for all other elements (from 72 to 66 at %). A subtler but unmistakable trend that

emerges is the slight enrichment of Mo as well on the stacking fault, which is not as strong as Cr or Co due to lower concentration (~ 2 at %) in the alloy itself. Also can be seen in the line plot (Fig. 1b) , but barely noticeable in the composition map, is slight enrichment of W in the stacking fault. These profiles, which were obtained across the stacking faults, do not indicate evidence for elemental denuded zones adjacent to the faults.

For the CMSX-4 sample, the microstructure of the alloy is populated with numerous dislocations and stacking faults in both the matrix and precipitate phases. The majority of the stacking faults in the γ' lie on the primary (1-11) slip plane which are viewed edge-on in HAADF and for EDS analysis. An example of a compositional mapping obtained at significantly lower magnification than that presented above is shown in Fig. 2, where three faults are observed traversing a large γ' precipitate. Note that the bottom left-hand corner of the maps includes a small region of the γ channel. Once again, it is apparent that the segregation of Cr and Co is occurring, while Ni and Al concentrations are lower at the faults. In this analysis, segregation of the heavier elements in this alloy (Mo, W, Ta and Re) is not detected. It is also noteworthy that the faults within the gamma prime are quite long (> 200nm) because of the larger size of the primary γ' precipitates. Quantitative chemical profiles obtained parallel to the fault plane are shown in Fig. 3. More detailed analysis (not shown here) has shown that the compositions of the principal elements (Co, Cr, Ni and Al) are essentially invariant along the faults. This observation provides additional insight into the possible diffusion mechanism involved in the sharing process, as discussed below.

This study for the first time has established that there exists significant compositional variation associated with stacking faults created following intermediate temperature deformation of two commercial superalloys. The elements that are seen primarily richer on the fault itself are Co and Cr. In alloy ME3, there is some evidence for slight enhancement of Mo at the faults, while there is presently no indication of heavy element segregation or departioning in CMSX-4.

The result that there is little or no heavy element segregation to the faults is a surprising result when considering the enhanced HAADF intensity that is characteristically observed at stacking faults and deformation twins in the g' phase of these superalloys. The question is whether the enhanced intensity can be understood on the basis of these new EDS results. Shown in **Table 1** are atomic percent (and fraction) values for each of the elements obtained via EDS analysis at a stacking fault versus in the adjacent matrix based on the quantitative analysis shown in Fig. 1. These values have been obtained by averaging the composition in a narrow rectangular region (dimensions 7 nm wide by 2 nm long) parallel to the fault. Using the atom fraction for each element, an "average" atomic number corresponding to each region has been calculated. It can be seen that indeed the average atomic number at the stacking fault (27.4) is larger than that in the adjacent matrix (26.6). While this is not a large difference, it is consistent with the contrast observed in HAADF images, where the image intensity scales approximately as the $Z^{\sim 1.7\text{-}2}$. Apparently the loss of Ni and Al from the fault region is sufficiently offset by the gain in Co, and to a lesser extent Cr, to result in a net gain in average atomic number.

There has been previous work on Suzuki segregation occurring where solute elements preferentially segregate to the extended stacking faults in several alloys. For example, a higher concentration of Si is seen at stacking faults in a Cu-Si alloy, leaving behind a Si denuded region adjacent to the fault. Han and Jones [12] have shown that wider and higher numbers of stacking faults occur after deformation at higher temperature as compared to room temperature deformation in a Co-Ni-Cr-Ni based superalloy. These authors have interpreted this effect in terms of Suzuki segregation where increased solute levels (mostly Mo, Al and occasionally Ti and Nb) were measured at the stacking faults. In general, it is speculated that the primary driving force for this segregation is to lower the stacking fault energy. The hypothesis is that elements that make the HCP structure more stable relative to FCC should segregate to the stacking faults, which locally have an HCP structure.

On the other hand, Koizumi at al [13] have shown that extended SFs are produced in the fcc phase of Co-Ni based superalloys when Nb is added in excess of 2% and following static annealing. Phase field simulation by the same authors has suggested that elements such as Co, Cr, Nb and Mo would have greater affinity for SFs when compared to Ni. However, decisive experimental evidence is still lacking in terms experimental measurement of specific elements segregating to the SF.

The segregation patterns in this study are very intriguing. First of all, the stacking faults exhibiting segregation in this case are in the γ' ordered phase where there exists already a strong tendency for alloying elements to prefer specific atomic lattice sites. Thus, there is not only a structural component to the fault energy, but formation of high-energy nearest-neighbor configurations can also strongly influence the fault energies. The energy penalty varies depending on the type of stacking fault. For simplicity, consider the case of stoichiometric, ordered $Ni_3Al$ as the γ' phase. In this case, an SISF created by the shearing of a 1/3<112> superatial dislocation will yield a purely structural fault where the stacking sequence is disturbed, but no high energy Al-Al nearest-neighbors are formed. However, shearing the same structure with a 1/6<112> Shockley partial will create a complex stacking fault (CSF) fault with the formation of numerous, high energy Al-Al nearest-neighbors. Likewise, two Shockley partials traveling on adjacent {111} planes would form a two-layer CSF with even higher energy. The concept of "reordering" was introduced to explain how elementary 1/6<112> partial processes could nevertheless result in the formation of low energy faults [Kolbe]. For instance, a two-layer CSF can reorder into a low energy superlattice extrinsic stacking fault (SESF) through local, vacancy-mediated diffusional pathways. One possible source for these two-layer SESFs is illustrated in Fig. 3a where it is envisioned that two matrix ½<110> dislocations approach each other at the γ/γ' interface, then the leading partials cooperatively shear the g' precipitate. The faults studied in this work are SISFs, which can also be created with the assistance of reordering by the coordinated movement of three Shockley partials on two planes that geometrically would create a CSF on top of an APB. This process is discussed in detail in Voronstov, et al [9]. Once again, this fault combination produces wrong nearest neighbors that can be eliminated via reordering. High resolution HAADF observations indicate that this two layer configuration of Shockley partials is indeed responsible for SISF formation at intermediate

temperatures in CMSX-4 [9]. Therefore, potentially of relevance to the formation of SISFs are also the CSF and APB energies that may be precursors to the SISF prior to reordering.

Karthikeyan, et al. [14] has also explored the effect of ternary alloying additions on varies faults in the g and g' phase of Ni-based superalloys. The effect of ternary additions of Ti and Ta on the Al sublattice, as well as Ni sites on the Al sublattice were explored. It was found that Ti and Ta tended to increase SISF and more strongly APB and CSF energies. It was argued that Ni-Ti and Ni-Ta bonds have high energy. Conversely, Ni antisites tended to decrease all the fault energies since Ni-Al bonds are of low energy. If the segregation behavior observed in the present study is associated with lowering the energy of the stacking faults, these calculations do not shed light on this behavior. For instance, Ni is clearly reduced at the faults, although the Ni content is below the stoichiometric value of 0.75. The strongly segregating species of Cr and Co were also not considered in their study since these elements partition strongly to the g phase, and thus should be of less importance to faults in the g' phase. Thus, this particular set of calculations is not necessarily relevant to the case of these two commercial alloys that are more compositionally complex than the ternaries considered.

A rudimentary explanation for the observed segregation behavior is obtained by simply noting that the local composition of the faults is closer to that of the g phase. Therefore, a reasonable hypothesis is that the fault energy is being lowered by the local compositional changes. However, if it is assumed that SISFs are formed via a pure shear process involving 1/3<112> superpartials, the driving force for segregation is not obvious. The SISF has the lowest energy of the planar faults in the $\gamma'$ structure, and does not have first or second nearest neighbor violations. Therefore, there would be little driving force to lower its energy by incorporating g-forming elements. On the other hand, the SISF formed by the reorder-mediated process, originating from a higher energy fault configuration such as an APB/CSF structure, would be able to lower its energy significantly by creating a local chemistry similar to the $\gamma$ phase.

Another important question concerns the diffusion process itself. A better understanding of this process could provide a more quantitative description of the rate limiting behavior associated with g' shearing. Three possible scenarios for the source of Cr and Co, and depletion of Ni and Al, are illustrated in Fig. 4. In the first scenario, it can be postulated that diffusion occurs perpendicular to the faults. In this case, since the diffusing elements would originate from the adjacent $\gamma'$ phase, it might be expected that Ni and Al could "pile-up" near the faults while Co and Cr might be depleted parallel to the faults. However, there is presently no evidence for these features based on the present EDS results, such as the lateral compositional profiles in Fig. 1b.

A second possibility is that diffusion occurs parallel or along the faults, with Co and Cr diffusing from the g channel, while Ni and Al diffuses to the channel. However, in this case the diffusion distances for these elements must be consistent with the length of the faults observed in the $\gamma'$ precipitates. Taking the case of CMSX-4 and the corresponding Super-X map shown in Fig. 2b, this creep test was conducted at 850°C for 8 hrs, after which time the

sample was quickly cooled under load. Using Thermocalc and the mobility database MOBNI2 that is developed to address the diffusion problem in the ordered phase for Ni-based superalloys, the diffusion coefficients for each element, and the corresponding diffusion distances (estimated as $(Dt)^{1/2}$) for the time scale of this creep test are shown in **Table 2**. Of the four major participating elements, Al has the longest diffusion length of 170 nm, while Ni has the shortest at 10 nm. However, the faults seen in Fig. 2 are on the order of 200nm long, and even longer faults have been observed in this sample, where the average γ' precipitate size is 300 nm [check with Cathie]. Therefore, diffusion in the bulk would not be fast enough to enable formation of the local compositions exhibited by these extended faults. Furthermore, as shown in Fig. 2b, there appears to be no indication of varying elemental concentration along these faults, as might be expected if this is due to diffusion from the g channel.

A third possibility is that there is indeed diffusion to/from the γ channels, but that it occurs along the dislocation lines of the shearing partials, as shown in Fig. 4c. This is an interesting possibility since the diffusion rates (and distances) would be greatly accelerated relative to bulk diffusion. The partial dislocations responsible for creating the fault therefore may also provide natural conduits for flow of atomic species necessary to lower the energy of the faults and enable shearing to take place.

In actuality, both reordering and long-range diffusion may be occurring simultaneously in the shearing process. However, since reordering requires atomic movements over only short distances of the order of interplanar spacing, it might expected that the movement of partials is instead controlled by the rate of diffusion of segregating (and departitioning) elements. The present results demonstrating a clear compositional signature associated with the γ' shearing process fundamentally changes the perspective with regard to the rate limiting process associated with propagation of these faults.

## Conclusions

Needs to be written.

## References


1. Leverant GR, Kear BH, Oblak JM. The influence of matrix stacking fault energy on creep deformation modes in g' precipitation-hardened nickel-base alloys. Metallurgical Transactions 1971;2:2305
2. The role of stacking fault shear in the primary creep of [001]-oriented single crystal superalloys at 750°C and 750 MPa, C.M.F. Rae, N. Matan, R.C. Reed, Materials Science and Engineering: A, **300**, 1–2, 28 2001, P. 125–134

3. C.M.F. Rae, R.C. Reed, Primary creep in single crystal superalloys: Origins, mechanisms and effects, Acta Materialia, **55**, 3, 2007, p.1067–1081.
4. Kolbe M. The high temperature decrease of the critical resolved shear stress in nickel-base superalloys. Materials Science & Engineering, A: Structural Materials: Properties, Microstructure and Processing 2001;A319-321:383.
5. Microtwinning and other shearing mechanisms at intermediate temperatures in Ni-based superalloys, L Kovarik, RR Unocic, J Li, P Sarosi, C Shen… - Progress in Materials …, 2009 – Elsevier
6. Investigation of creep deformation mechanisms at intermediate temperatures in René 88 DT, GB Viswanathan, PM Sarosi, MF Henry, DD Whitis… - Acta Materialia, 2005.
7. Evaluation of the jogged-screw model of creep in equiaxed γ-TiAl: identification of the key substructural parameters, S Karthikeyan, GB Viswanathan, MJ Mills - Acta materialia, 2004.
8. The intermediate temperature deformation of Ni-based superalloys: Importance of reordering, L Kovarik, RR Unocic, J Li, MJ Mills - JOM, 2009.
9. High-resolution electron microscopy of dislocation ribbons in a CMSX-4 superalloy single crystal, V.A. Vorontsov, , , L. Kovarik, M.J. Mills, C.M.F. Rae, Acta Materialia **60**, 12, 2012, P. 4866–4878.
10. Need a reference here
11. Fine-scale structure of dislocations and debris in deformed Ni-based superalloy R104, P.J. Phillips, M.J. Mills - Philosophical Magazine, 2013, p. 82-95.
12. Direct evidence for Suzuki segregation and Cottrell pinning in MP159 superalloy obtained by FEG(S)TEM/EDX, G.W. Han, I.P. Jones ∗, R.E. Smallman, Acta Materialia 51 (2003) 2731–2742.
13. Suzuki segregation in Co–Ni-based superalloy at 973 K: An experimental and computational study by phase-field simulation, Y. Koizumi, T. Nukaya, S. Suzuki, S. Kurosu, Y. Li, H. Matsumoto, K. Sato, Y. Tanaka, A. Chiba, Acta Materialia 60 (2012) 2901–2915.
14. Effect of Off-Stoichiometry and Ternary Additions on Planar Fault Energies in Ni3Al, KV Vamsi, S Karthikeyan - Superalloys 2012, 2012

Table 1: Net atomic number averaged within narrow regions parallel to the fault and away from the fault shown in Figure 1.

| | **Al** | **Ni** | **Co** | **Cr** | **Ti** | **Nb** | **Mo** | **W** | **Ta** | **Average Atomic No.** |
|---|---|---|---|---|---|---|---|---|---|---|
| **Stacking Fault** | 5.8 | 66.3 | 12.9 | 2.7 | 8.6 | 0.9 | 1.3 | 0.7 | 0.8 | 27.36 |
| **Matrix** | 9.4 | 71.6 | 7.6 | 1.7 | 7.6 | 0.4 | 0.7 | 0.5 | 0.5 | 26.6 |

Table 2: Composition and diffusion coefficients in the g and g' phases based on the Thermocalc MobNi2 database. The diffusion distances (in nm) for each element in the g' phase for an 8 h period at 850°C (corresponding to the creep test resulting in the data shown in Figs. 2 and 3) are also shown.

| CMSX-4 | Ni | Cr | Co | Mo | W | Al | Ti | Ta | Re |
|---|---|---|---|---|---|---|---|---|---|
| Nominal | 60.8 | 6.5 | 9.6 | 0.6 | 6.4 | 5.6 | 1.0 | 6.5 | 3.0 |
| □′ | 71.73 | 2.03 | 3.93 | 2.48 | 2.46 | 8.13 | 1.51 | 9.85 | 1.10 |
| □ | 39.9 | 15.05 | 2.04 | 1.27 | 1.39 | 0.76 | 0.028 | 0.096 | 8.53 |
| □ LogD*($m^2$/s) | -20.4 | -18.7 | -18.7 | -21.4 | -22.3 | -18.0 | -20.4 | -21.6 | -19.8 |
| Distance (8h)/nm | 10.7 | 75.8 | 75.8 | 3.4 | 1.2 | 170 | 10.7 | 2.7 | 21.4 |
| □ LogD*($m^2$/s) | -19.5 | -17.9 | -18.0 | -18.1 | -19.1 | -17.3 | -17.2 | -17.8 | -19.7 |

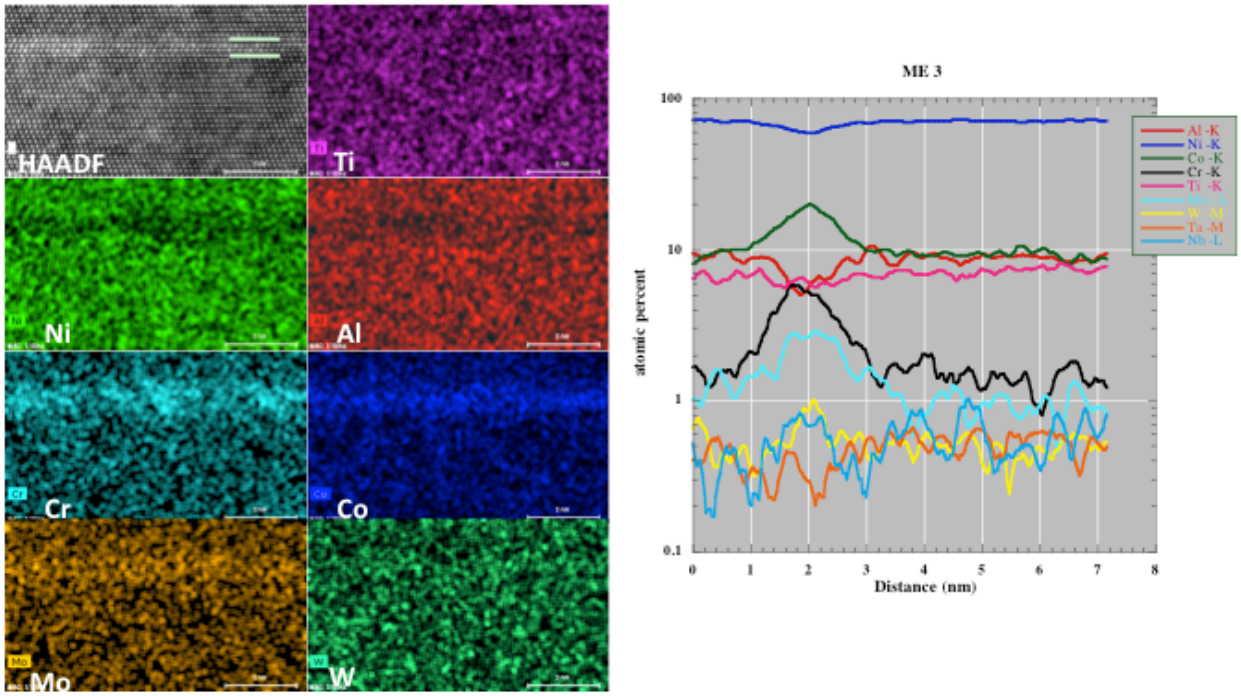


Figure 1 (a) Atomic resolution STEM HAADF image showing intrinsic stacking fault on edge in alloy ME3 and corresponding elemental maps and (b) plot of elemental variation normal to the stacking fault. The data is integrated over the entire length of the region shown in (a).

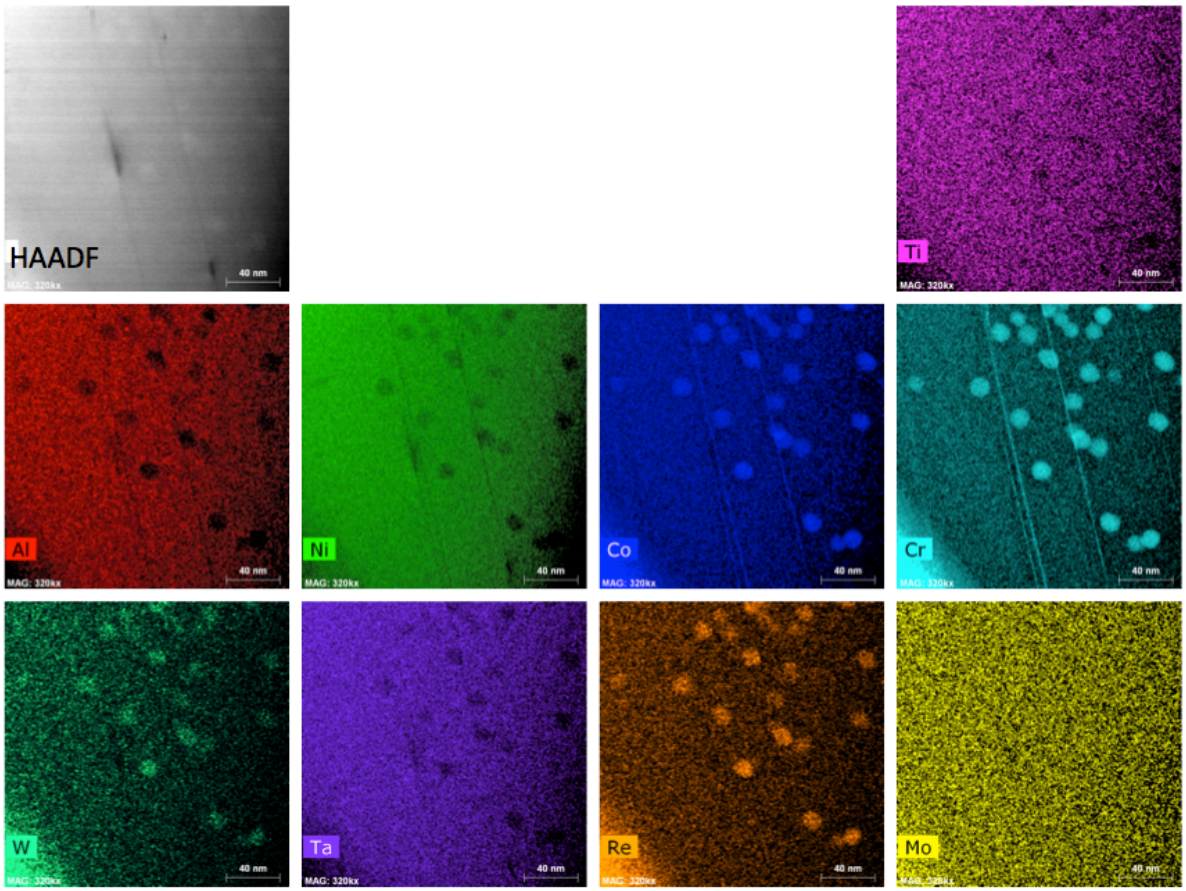


Figure 2: STEM HAADF image showing several stacking faults on edge in alloy CMSX4 and corresponding elemental maps.

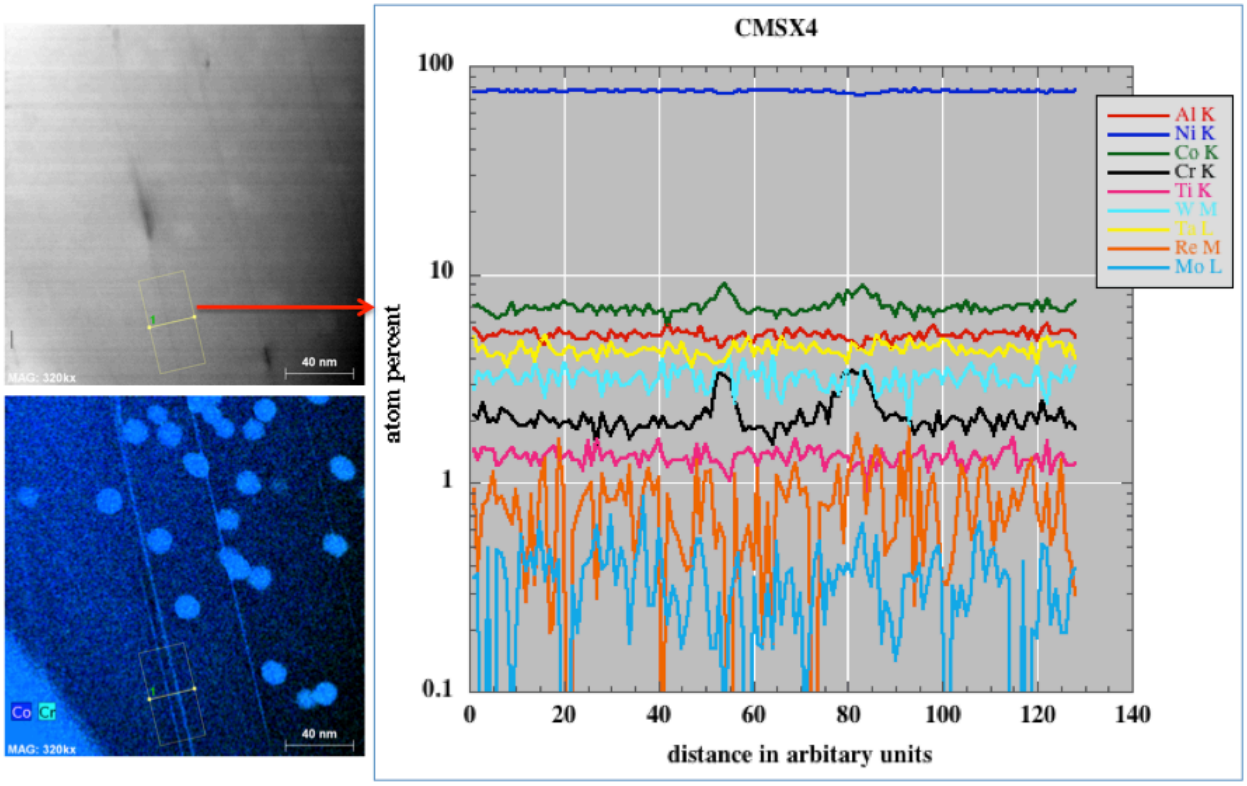


Figure 3: (a) STEM HAADF image showing the stacking fault on edge in alloy CMSX-4, (b) combined Co and Cr map and (c) plot of elemental variation normal to the stacking fault within the marked region in (a).

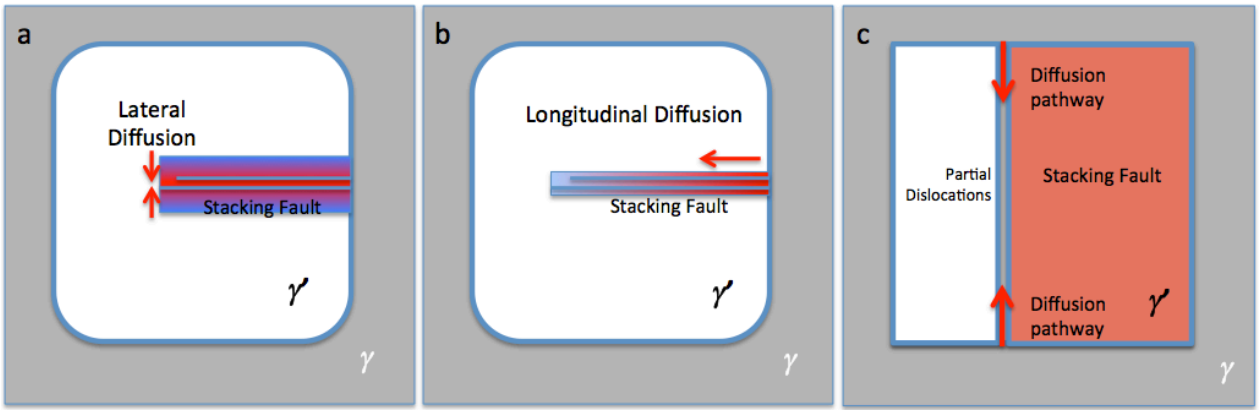


Figure 4: Illustrations of possible diffusion path scenarios for segregating elements (i.e. Co and Cr) originating from (a) lateral diffusion, (b) longitudinal diffusion and (c) pipe diffusion. Diffusion of Ni and Al would be in the opposite direction to those indicated.